Advances in Science and Technology Research Journal

Advances in Science and Technology Research Journal, 2026, 20(4), 160–177
https://doi.org/10.12913/22998624/214691
ISSN 2299-8624, License CC-BY 4.0

Received: 2025.10.28
Accepted: 2026.02.15
Published: 2026.03.01

Experimental and numerical study on the free vibrations of soda-lime-silicate float glass panes with three different thicknesses

Małgorzata Abramowicz[1*], Hanna Weber[1*], Marcin Kozłowski[2]

[1] Department of Theory of Structures, Faculty of Civil and Environmental Engineering, West Pomeranian University of Technology in Szczecin, al. Piastów 50a, 70-311 Szczecin, Poland
[2] Department of Structural Engineering, Faculty of Civil Engineering, Silesian University of Technology, ul. Akademicka 2A, 44-100 Gliwice, Poland
* Corresponding author's e-mail: mabramowicz@zut.edu.pl; weber@zut.edu.pl

ABSTRACT

This study investigates the free vibration behaviour of soda-lime-silicate float glass panes with different thicknesses through combined experimental and numerical analyses. Experimental modal analysis was conducted on three glass plates with dimensions of 400 × 800 mm and nominal thicknesses of 4, 8 and 12 mm. The tests were performed using an impact hammer and triaxial accelerometers positioned at 27 measurement points, enabling the identification of natural frequencies and corresponding mode shapes. To minimize the influence of boundary conditions, the panes were elastically supported at the zero-deformation points of the first flexural mode. The experimental results were compared with numerical simulations performed in ABAQUS using two finite element formulations: quadrilateral shell elements and 3D solid elements with incompatible modes. A systematic mesh-refinement study was carried out to determine the relationship between element size, computational time and result accuracy. The analysis showed that for both element types, the frequency results converge when the finite element size is approximately equal to the pane thickness. Modal assurance criterion (MAC) analysis confirmed a high correlation between experimental and numerical mode shapes, with diagonal MAC values approaching unity. The differences between experimental and numerical results decreased with increasing glass thickness, reaching below 2% for the thickest plate. Overall, shell models provided accuracy comparable to solid models while reducing computational time by an order of magnitude. Therefore, shell elements are recommended as an efficient and reliable tool for the modal analysis of glass panes.

Keywords: glass structures, modal analysis, finite element method, numerical modelling, parametric analysis.

INTRODUCTION

All structural elements exhibit high vibration amplitudes when subjected to dynamic loads. In this context, modal analysis is an effective method for identifying the dynamic properties of structures, enabling the determination of modal parameters such as natural frequencies and mode shapes [1]. Knowledge of these parameters is particularly important for the structural design and assessment of components made of glass due to its fragile nature, brittleness, slenderness and tendency to fracture under dynamic loads [2]. In addition, reliable dynamic analysis is essential for numerical modelling, which is widely used in engineering practice and requires accurate representation of materials, boundary conditions and model validation.

Existing research on the dynamic behaviour of glass structures has been focusing mainly on laminated or assembled glazing systems used in façades, protective glazing and architectural applications. Prior studies have examined impact resistance, seismic response and vibration mitigation, whereas investigations into the free vibration characteristics of monolithic soda–lime–silicate

float glass are considerably less common. For instance, Chaparala et al. [3] and Fröling et al. [4] analysed the dynamic response of glass under impact loading using experimental methods and finite element simulations. Their results highlighted the relevance of strain measurement techniques, such as digital image correlation and introduced simplified numerical models capable of predicting stress and deflection under various support conditions. The influence of boundary restraints on the vibration parameters of glass panels was examined by Bedon et al. [5], who showed that support flexibility significantly affects natural frequencies and damping. Similar techniques were applied at a structural scale by Bedon and Bergamo [6], who used operational modal analysis for vibration-based condition assessment. Broader system-level investigations, such as those by Bedon and Amadio [7, 8], explored glazing façades as active vibration-control elements, introducing the concept of distributed tuned mass damping under extreme loading scenarios.

In summary, the existing literature primarily addresses laminated or multi-layer glazing subjected to impact, seismic or environmental loading. Research explicitly targeting the intrinsic vibration characteristics of monolithic soda–lime–silicate glass and in particular their dependence on thickness, remains limited. This highlights a clear research gap concerning the systematic identification of fundamental modal properties of monolithic glass under controlled boundary conditions. Furthermore, many published modal studies rely on single-point vibration measurements, which do not capture the global dynamic response of the panel and limit the identification of mode shapes [9, 10]. In addition, damping is typically omitted due to the inherently low energy dissipation of glass. Although this effect is minor [11], a nominal viscous damping ratio of approximately $\xi \approx 1\%$ is often assumed in dynamic analyses of glass structures [5, 12].

To address the identified gap, this work performs an experimental modal analysis using an impact hammer and multiple accelerometers on float glass plates of varying thicknesses. The experimental results are subsequently compared with numerical simulations. The study constitutes the first stage of a broader research programme dedicated to developing a comprehensive analytical and numerical model of monolithic glass plates. The motivation behind this investigation is to determine how the vibration frequency values associated with individual modal shapes evolve with glass thickness and to identify which numerical modelling approach best reproduces the experimentally observed dynamic behaviour. These questions are central to improving the predictive capability of dynamic simulations of glass structures.

The dynamic response of any structural system results from the superposition of multiple vibration modes. While the finite element method (FEM) allows detailed dynamic simulations, its computational cost increases with mesh refinement and model complexity. Simplified analytical approaches offer faster computation, either by assuming a dominant vibration mode or by representing a reduced multimodal response. These simplifications, however, may affect accuracy. The present experimental modal analysis is therefore used to validate the corresponding numerical models. In subsequent stages of the project, the identified frequencies will support the development of analytical procedures for impact simulations, aiming to achieve dynamic responses comparable to FEM at a significantly reduced computational cost.

MATERIAL AND METHODS

Materials

In the research, commercially available soda–lime–silicate float glass, which is the primary glass used in construction [13], was considered. According to the material standard PN-EN 572-1 [14], soda–lime–silicate glass has a density of 2500 kg/m³, a Young's modulus of 70 GPa, and a Poisson's ratio of 0.2. However, literature reports Young's modulus values in the range of 68–74 GPa [15, 16 and 17]. The Poisson's ratio is also reported to differ, with a value of 0.23 in design standards for structural elements made of glass (PN-EN 16612) [18].

Due to the nature of the investigation and the need to minimize the risk of fracture when impacted with a modal hammer, tempered glass was selected because it offers nearly three times the strength of annealed glass [19]. Although the tempering process introduces compressive surface stresses, it does not alter the fundamental physical properties governing dynamic behaviour, such as Young's modulus, Poisson's ratio or the density of soda-lime-silicate glass. Consequently, tempering has no meaningful influence on the modal properties of the tested panes.

Test specimens

In this study, three float glass panes measuring 400 × 800 mm with nominal thicknesses of 4, 8 and 12 mm were used. Due to the significant sensitivity of modal analyses to the physical parameters of the tested elements, the samples were subjected to precise measurements of their dimensions, thickness and mass. Special attention was given to the actual thickness of the panes, as it may differ from the nominal value provided by the manufacturer. Each specimen was cut from a jumbo float-glass plate of 3210 × 6000 mm. Since the float process ensures a highly uniform thickness across the entire pane, the values measured at the edges are representative of those in the central region. For each pane, 24 measurements were taken along the edges using a micrometre screw. Subsequently, based on the precise volume and mass data, the specific weight was calculated. When comparing the actual and theoretical mass (calculated on the basis of nominal dimensions and nominal specific weight), it was found that, on average, the former was 3.9% lower. Similarly, the measured specific weight was 1.9% lower than the nominal value.

An overview of the specimens and their physical parameters is given in Table 1. The values presented in Table 1 (average thickness and mass) were calculated separately for each plate, whereas the specific weight, since the glass originated from the same production batch, was calculated based on all measurements. The "±" symbol appearing in Table 1 indicates the standard deviation. The column reporting the measured average thickness of the samples indicates that as the thickness of the glass pane decreases, the absolute difference between the nominal and actual thickness increases. This difference may result from technological limitations in the glass-forming process, in which maintaining uniform thickness is more difficult for thin plates due to their higher susceptibility to local deformations and nonuniform cooling during production.

Test set-up and testing procedure

The test set-up (Figure 1a) was carefully designed to minimize the influence of boundary conditions on the results of the modal analysis. The glass specimen was supported at four points, located 180 mm from the long edges and 100 mm from the short edges of the plate (Figure 2). The positioning of these supports was determined by the location of the inflection points for the first significant flexural vibrations (zero-deformation points). The glass panes were supported at the nodal points of the first flexural mode in order to minimise the effects of the boundary conditions on the fundamental vibration. The largest displacements occur in the first mode, while the amplitudes of higher-order modes decrease significantly. This means that the influence of the supports on higher-order modes is minimal. The supports consisted of steel springs with a stiffness of 1.19 kN/m. Wooden pads and EPDM rubber layers were placed on the springs. The EPDM pads were not bonded to the glass surface, allowing localised separation of the specimen from the supports. The springs were mounted in sockets rigidly fixed to the base plate.

To measure accelerations on the specimen, 27 measurement points were defined, arranged in three rows of nine points each. Since only nine PCB 356A01 triaxial accelerometers, each weighing approximately 1 g, were available, the experiment was repeated three times by relocating the accelerometers row by row, from the bottom to the top (see Figure 2b). The mass of the accelerometers (1 g) is negligible compared to the glass panes (3.04, 6.37 and 9.60 kg for 4, 8 and 12 mm thickness, accordingly), and therefore their influence on the dynamic response is insignificant.

Additionally, to validate the measurement data, a non-contact laser displacement sensor, optoNCDT ILD1420 (measurement range: ±25 mm with an accuracy of 0.04 mm) was mounted beneath the specimen. The sensor measured the

Table 1. Overview of specimens

Description of the glass plate	Nominal thickness [mm]	Measured average thickness [mm]	Measured mass [kg]	Specific weight of glass [kN/m^3]
400 × 800 × 4	4	3.79±0.01	3.04	24.53±0.06
400 × 800 × 8	8	7.92±0.09	6.37	
400 × 800 × 12	12	12.01±0.03	9.60	

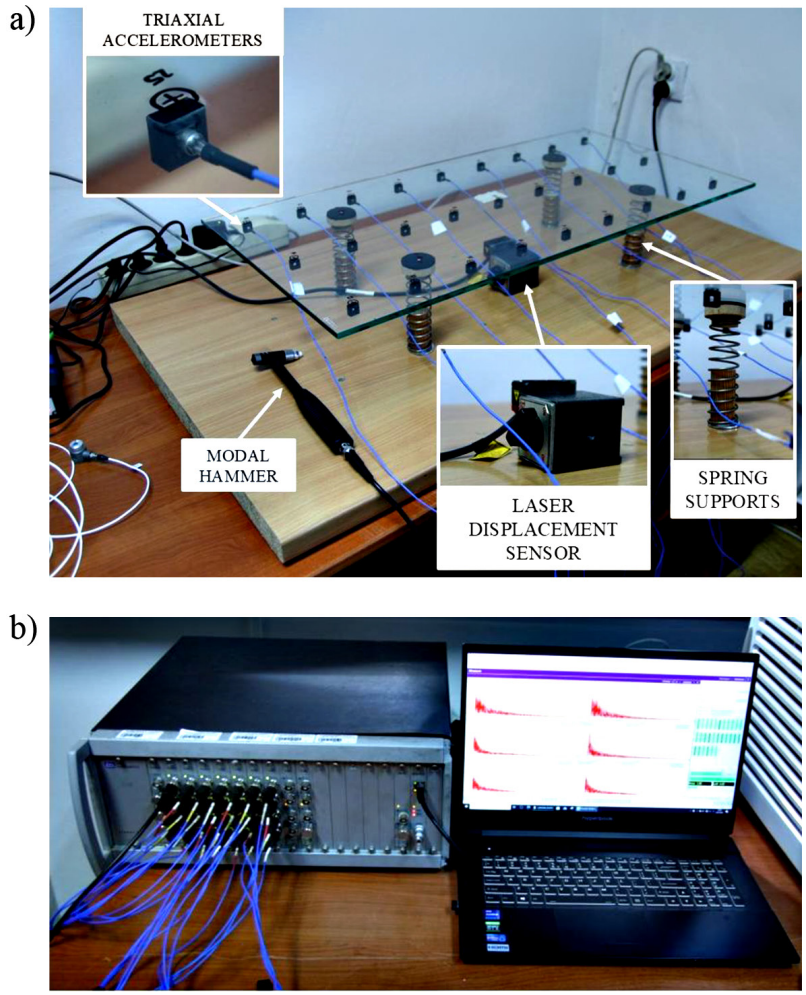

Figure 1. Laboratory test: (a) research station; (b) the analyser LMS SCADAS

displacement of the lower surface of the specimen at its central point during testing.

The glass pane test involved applying force with a PCB 086C01 modal hammer (PCB Piezotronics, Depew, NY, USA) and recording the resulting acceleration response, by using PCB 356A01 triaxial accelerometers (PCB Piezotronics, Depew, NY, USA). The signal was then processed using an LMS SCADAS III analyser (Siemenes, Planto, TX, USA) [20] and recorded on a computer using Test.Lab 2019.1 software (Siemens, Munich, Germany) presented in Figure 1b.

In the experiment, the dynamic response of the glass plates was measured using a standard modal analysis procedure. To ensure accurate and reproducible results, the following measurement and signal processing settings were applied: the frequency response function (FRF) was estimated using the H_1 estimator and the modal parameters were identified using the PolyMAX algorithm as implemented in the Siemens Test.Lab software (version 2019.1). The frequency resolution was set to 0.5 Hz, the acquisition time was 2 s per measurement. The pane was excited at three different locations (14-Z, 26-Z and 27-Z; Figure 2b) in order to obtain the widest possible range of natural mode shapes (flexural, torsional etc.). To ensure the statistical reliability of the results, the impact was repeated five times for each measurement row. In Test.Lab programme, each measurement was defined as one run. After completing one measurement line with three excitation points, the next measurement line was selected. In total, 9 runs were recorded for one glass plate in the programme. Next, using the Test. Lab software, a modal analysis was performed to identify the natural vibration frequencies and the corresponding mode shapes.

Methodology

To verify the accuracy of the model tuning, we compared the agreement between the natural vibrations obtained through experimental testing for the selected excitation point and those

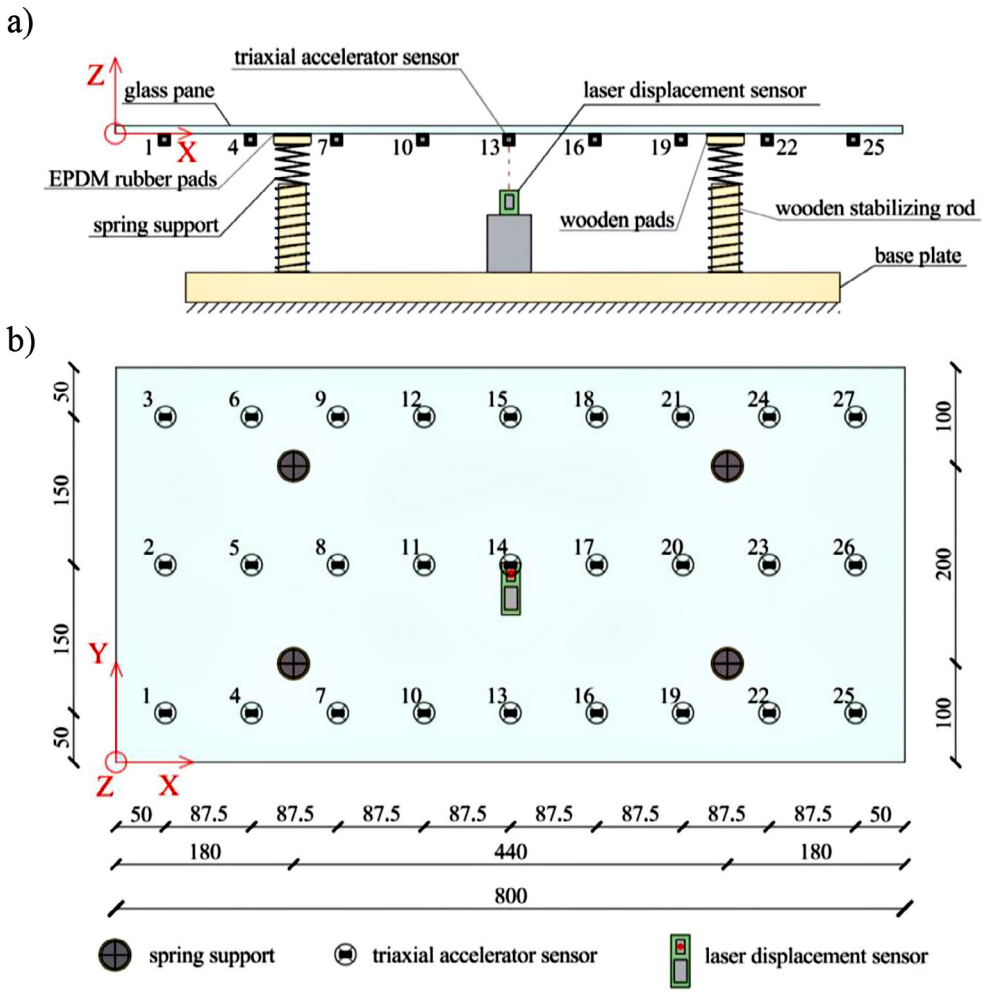

Figure 2. Research station: (a) front view, (b) glass plane top view

obtained from the numerical model. The accuracy of this agreement was verified, using the modal assurance criterion (MAC) [21, 22, 23]. The MAC value was calculated using the following formula:

$$\mathrm{MAC} = \frac{|\boldsymbol{\phi}_{exp}^{T}\boldsymbol{\phi}_{num}|^{2}}{\boldsymbol{\phi}_{exp}^{\mathrm{T}}\boldsymbol{\phi}_{exp}\boldsymbol{\phi}_{num}^{\mathrm{T}}\boldsymbol{\phi}_{num}} \tag{1}$$

where: ϕ_{exp} – the modal vector for the results of experimental research, ϕ_{num} – the modal vector for the results from numerical model.

When the MAC value approaches 1, it signifies a high level of agreement. Conversely, when the MAC value tends to 0, it indicates poor correlation. In the literature, a MAC higher than 0.8 indicates good correlation [24]. The MAC result is a square matrix, for which the diagonal is the MAC value for the mode shapes being verified.

In order to compare the vibration frequencies obtained in the experimental measurements and numerical simulations, the relative error parameter Δ was calculated according to the equation:

$$\Delta = \left(\frac{f_{exp} - f_{\mathrm{num}}}{f_{exp}}\right) \cdot 100\% \tag{2}$$

This allows assessing how accurately the numerical model reflects the actual behaviour of the system.

Numerical model

A characteristic feature of a glass plate is its small thickness compared to the spatial dimensions. For this reason, shell elements with the same thickness as a glass pane are very often used in numerical modelling. They are characterized by a much shorter computation time compared to solid models and ensure computational accuracy [25]. In the case of static loads, the selection of shell elements gives relatively good agreement with reality [26], however, for dynamic analysis this issue requires verification.

This paper aims to investigate how the type of finite element and its size affect the results of modal analysis, i.e., frequency values and modal shapes. The study compared the results obtained for numerical models, performed using ABAQUS software, constructed from two types of meshes: quadrilateral shell element (S4) and 3D linear solid brick element with incompatible modes (C3D8I) [27]. The first one has 4 nodes and 6 degrees of freedom (DOF) in each of them (three mutually perpendicular translations and three angles of rotation, one relative to each axis) and is a frequently used finite element in the analysis of glass plates, especially due to the significantly shorter calculation time compared to solid ones. The second type is a solid element with 3 degrees of freedom (three mutually perpendicular translations) at each of eight nodes and 13 additional variables relating to the incompatible modes. This type of element is particularly suitable for thin plates where bending is dominant, as they improve their performance by reducing the locking effects characteristic of lower-order elements. The main goal of the numerical analysis is to find a model that provides correct modal results, validated against experimental results, in a relatively short time. Therefore, C3D8I elements were chosen over higher-order C3D20 elements (twenty-node brick element with quadratic interpolation), as they show good computation accuracy and significantly lower computational cost. Furthermore, owing to the incompatible modes, they avoid incorrect results related to the elements over-stiffening in FEM analysis, which could occur with the C3D8 elements.

The three glass samples analysed in the experiments came from the same batch, therefore, the same material characteristics were used in all numerical models, i.e., elastic modulus of E = 70 GPa, Poisson's ratio υ = 0.23 and density ρ = 2500 kg/m^3, based on standards PN-EN 572-1 [14] and PN 16612 [18].

Since the three considered plates had the same dimensions of 400 × 800 mm and differed only in thickness, the maximum finite element size of 40 × 40 mm was adopted for the analysed meshes in order to obtain at least of 10 finite elements along the shorter edge of the model. The mesh was then gradually refined in each model to examine the influence of the finite element size on the modal analysis results. Consequently, seven groups of finite element mesh densities with dimensions of 40 × 40 mm, 30 × 30 mm, 20 × 20 mm, 12 × 12 mm, 8 × 8 mm, 4 × 4 mm, and 2 × 2 mm were analysed. As a result, 14 numerical models were developed for each of the three analysed plates, 7 based on shell elements (S4) and 7 using solid elements (C3D8I) (compare with Figure 3).

The S4 elements were assigned the actual plate thicknesses, i.e., 3.79 mm, 7.92 mm, and 12.01 mm (see Table 1). In the case of solid models, the plates were divided into four C3D8I elements according to their actual thickness. However, for clarity of presentation, the element sizes in Figures 5–6 have been rounded to whole millimetres.

This approach ensured us to obtain the same number of finite elements in models with the selected mesh densities for all three plate thicknesses, as summarized in Table 2.

However, the computational time for the same meshes varied slightly depending on the sample; therefore, Table 2 shows the average time required to run the analyses for a given mesh, determined as the arithmetic mean of the results obtained from the three considered plates. The numbers of finite elements, nodes, and degrees of freedom (DOF) increase with the mesh density and are significantly higher for solid models than in shell models (see Table 2).

It should be noted that the computational time increases almost exponentially with the number of degrees of freedom, as shown for both analysed elements in Figure 4. For clarity of presentation, the horizontal axis shows the decimal logarithm of the number of degrees of freedom, denoted as Log(NDOF). As can be seen in Table 2, for a 40 × 40 mm mesh, the time required to conduct the modal analysis is approximately 1.5 times longer for C3D8I elements compared to shell ones, whereas for a 2 × 2 mm mesh, the time is already over an order of magnitude higher. The aim of this section is to identify an optimal numerical model for modal analysis, combining two basic criteria: result accuracy and low computation time.

First, for each glass pane, an analysis was performed to determine the convergence of the results obtained for the natural frequencies for individual mode shapes depending on the assumed finite element mesh density. The obtained results are presented in Figure 5 for shell models and in Figure 6 for solid ones. Each of the diagrams shows the percentage differences in the results obtained between two adjacent models with respect to mesh density. For example, the line corresponding to the 30 × 30 mm mesh shows the percentage difference between the results

Table 2. Main parameters of numerical models

Mesh [mm]	FEM elements number	Nodes number	NDOF	Log(NDOF)	Mean computational cost [s]
Shell elements					
40 × 40 × t	182	211	1266	3.10	1.43
30 × 30 × t	394	437	2622	3.42	1.53
20 × 20 × t	798	856	5136	3.71	1.80
12 × 12 × t	2115	2213	13278	4.12	2.73
8 × 8 × t	5007	5157	30942	4.49	4.97
4 × 4 × t	20412	20713	124278	5.09	17.97
2 × 2 × t	80911	81508	489048	5.69	78.07
Solid elements					
40 × 40 × t/4	720	4645	27870	4.45	2.20
30 × 30 × t/4	1568	10015	60090	4.78	3.50
20 × 20 × t/4	3085	19578	117470	5.07	5.77
12 × 12 × t/4	8704	54895	329370	5.52	15.27
8 × 8 × t/4	20000	125755	754530	5.88	34.63
4 × 4 × t/4	81069	508198	3049190	6.48	160.10
2 × 2 × t/4	321600	2013015	12078090	7.08	815.03

Note: where *t* denotes the thickness of the considered plate.

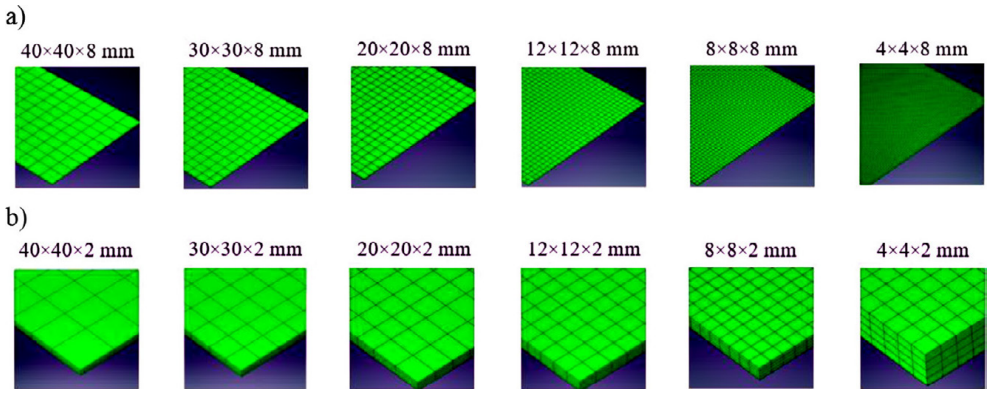

Figure 3. View of finite element meshes analysed in numerical models based on sample 400 × 800 × 8 mm (a) Shell models – elements S4, (b) Solid models – elements C3D8I

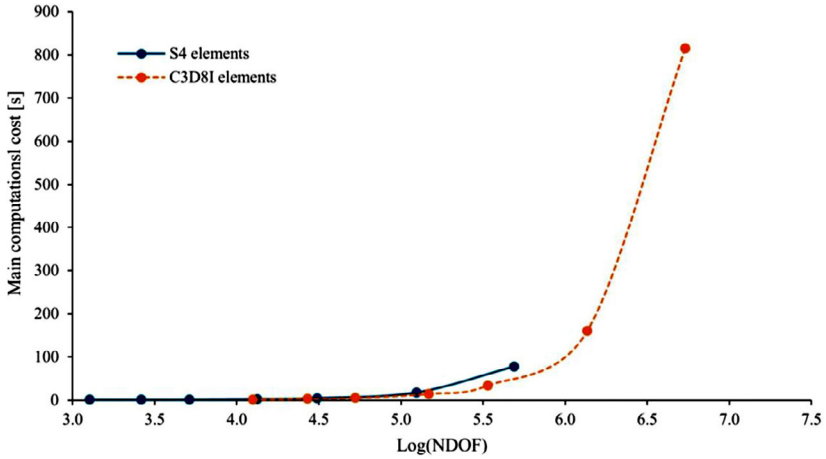

Figure 4. Comparison of numerical models using shell and solid elements – dependence between NDOF and computational cost

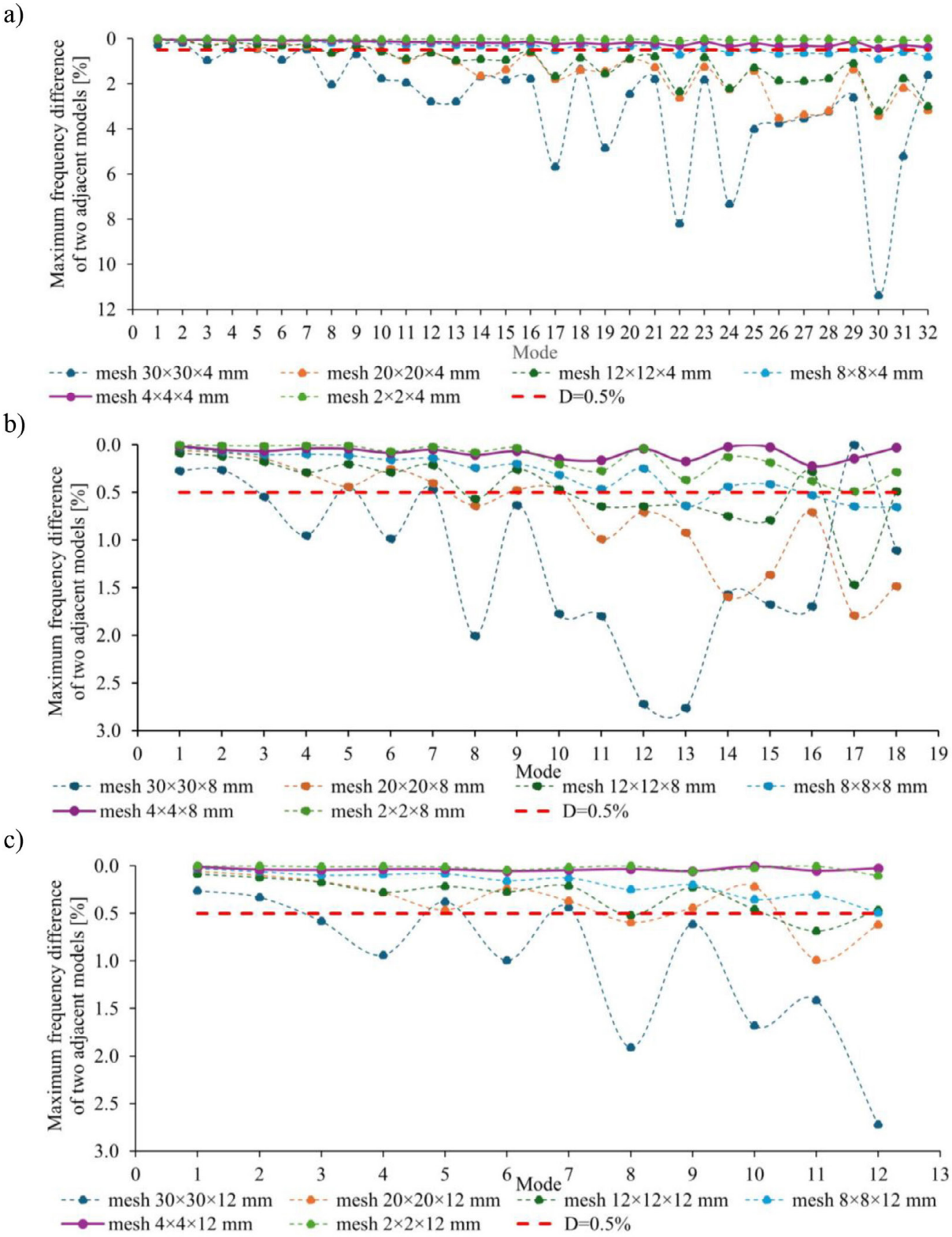

Figure 5. Analysis of the mesh size convergence of the shell numerical models: (a) Plate 400 × 800 × 4 mm, (b) Plate 400 × 800 × 8 mm, (c) Plate 400 × 800 × 12 mm

obtained for the 30 × 30 mm and 40 × 40 mm meshes, etc. Each diagram also includes a dotted red line indicating a 0.5% difference. The analysis of Figures 5–6 shows that regardless of the finite element used (S4 or C3D8I), the percentage differences in the obtained results decrease with an increase in both glass pane thickness and mesh density. The largest percentage differences

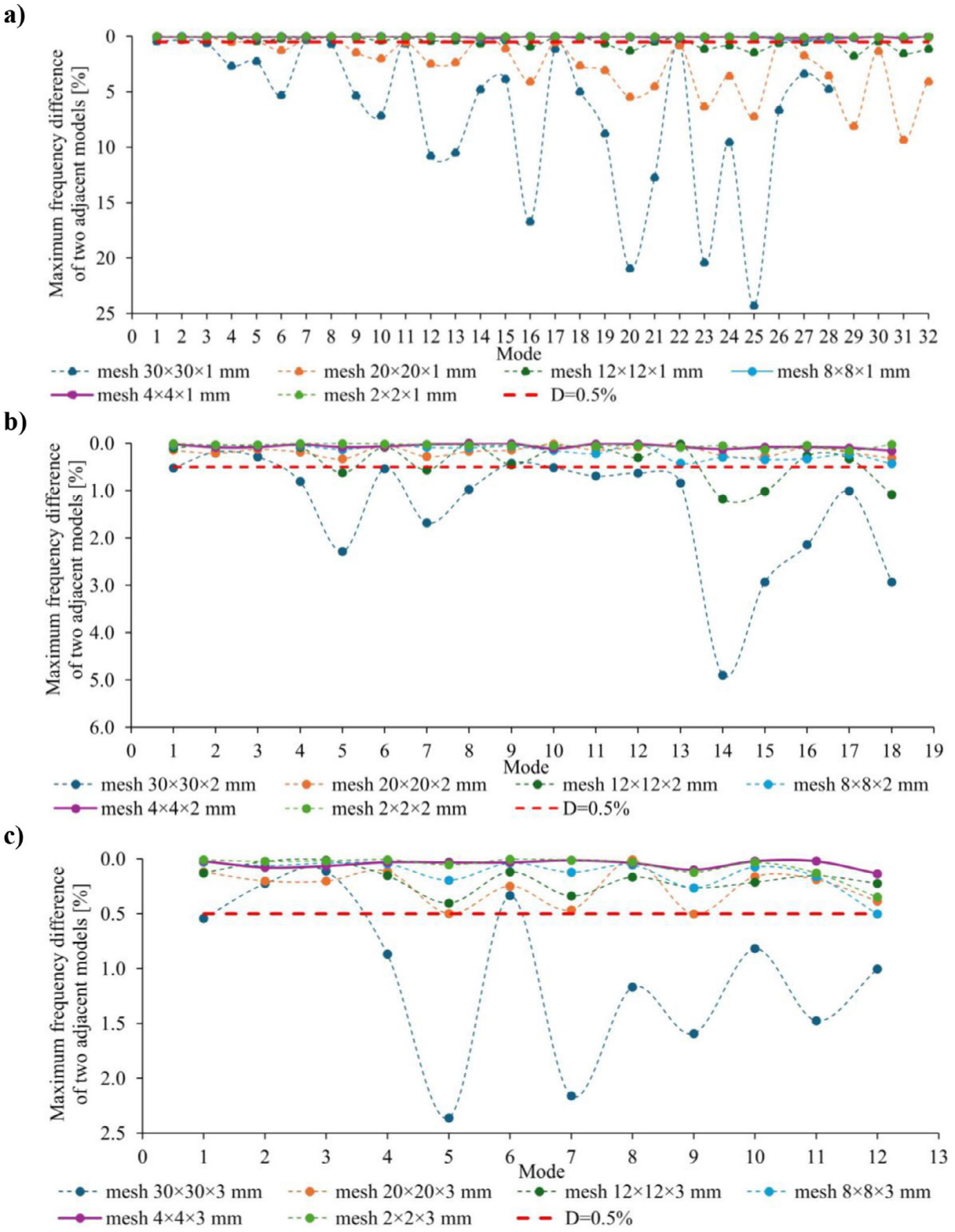

Figure 6. Analysis of the mesh size convergence of the solid numerical models: (a) Plate 400 × 800 × 4 mm, (b) Plate 400 × 800 × 8 mm, (c) Plate 400 × 800 × 12 mm

are obtained for the thinnest plate, which may be related to the large number of mode shapes that can be identified up to a frequency of 1000 Hz. Although the maximum percentage differences obtained for the coarsest meshes in solid models are higher than those in shell ones, C3D8I elements exhibit faster convergence during gradual mesh refinement compared to S4 elements.

However, this is associated with increased computation time. Based on the presented diagrams, it can be generally concluded that the minimum mesh size (regardless of its type, S4 or C3D8I) that yields result differences below 1% should be approximately equal to the glass plate thickness.

The convergence analysis was conducted to determine which numerical model should be used for the selected glass plates to compare with the experimentally obtained results. Figure 7 shows the convergence of the fundamental frequencies of the considered glass plates depending on the mesh density adopted during numerical computations and the type of FEM element used. As can be seen, in each case, an excessively large mesh in the shell model causes the obtained result to be overestimated, while in the case of the solid model, the opposite behaviour is observed. This pattern occurs analogously for each of the analysed frequencies, however, due to the limited scope of

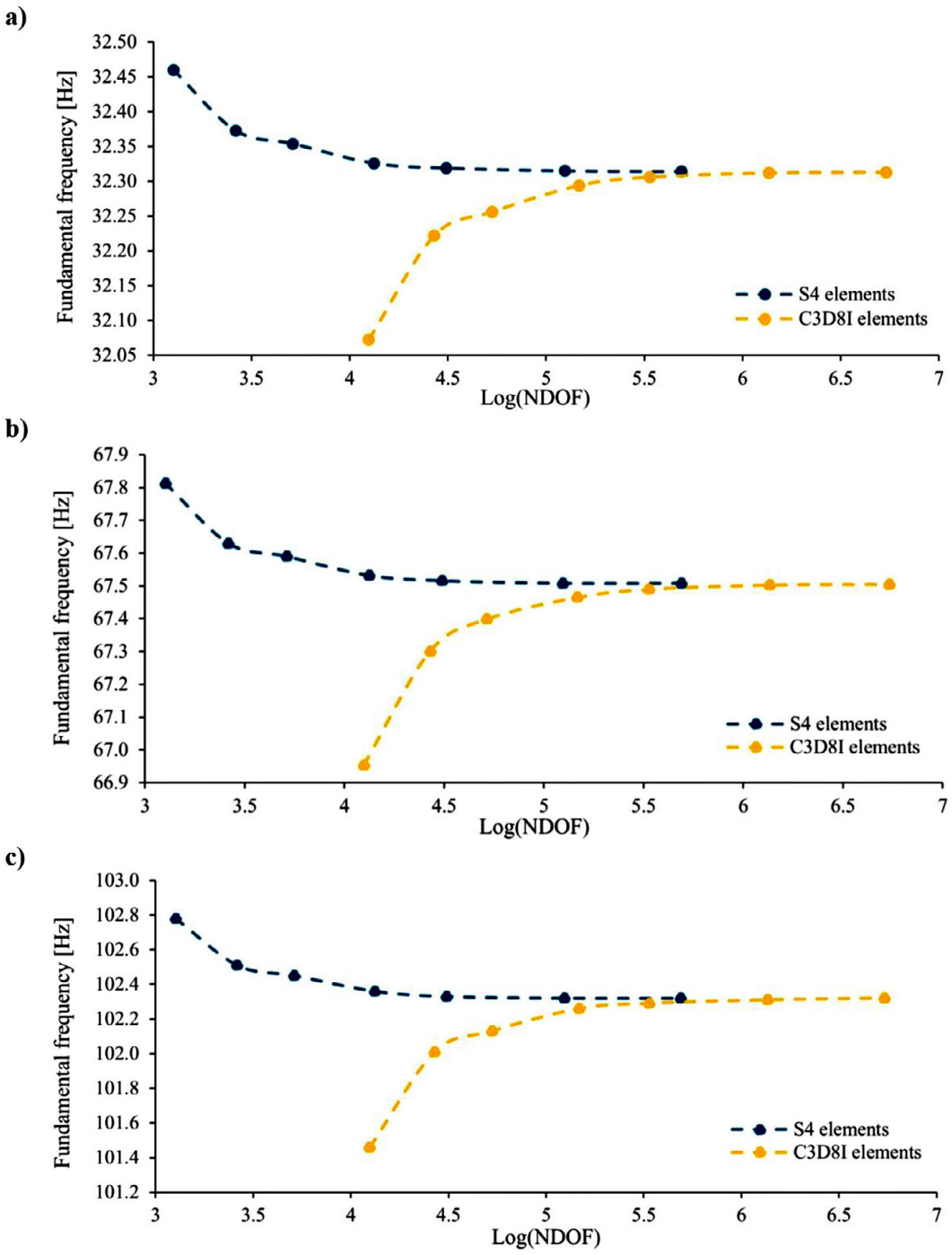

Figure 7. Comparison of the convergence of the numerical models on the example of the fundamental frequency: (a) Plate 400 × 800 × 4 mm, (b) Plate 400 × 800 × 8 mm, (c) Plate 400 × 800 × 12 mm

this paper, only the diagrams for the first mode are presented. Based on the obtained results, the models with meshes 4 × 4 mm were selected for comparison with the experiment for each of the considered plate, as they already provide accurate frequency predictions and require significantly less computation time in comparison to the mesh 2 × 2 mm. Figure 7 also shows that the frequency values obtained for both the 4 × 4 mm and 2 × 2 mm meshes are nearly constant on the horizontal line of the function illustrating the relationship between mesh size and the obtained frequency results. This, compared to the almost exponential relationship between computation time and mesh size (Figure 4), makes further mesh refinement uneconomical from a computational cost point of view.

In the numerical models developed in this study, damping was not included because the analysis focuses on the modal properties of the system. Modal analysis aims to determine the natural frequencies and corresponding mode shapes of an undamped structure; therefore, a damping coefficient was not applied.

RESULTS AND DISCUSSION

Experimental results

During the experiment, each of the three glass panes was subjected to a vertical force using a modal hammer at three consecutive points, i.e., in the centre of the plate (14-Z), at the edge of the specimens along the axis of symmetry (26-Z) and in the corner (27-Z). The individual locations are shown in Figure 3b. As a result of the test procedure described in section 2.3, acceleration values were obtained at 27 points under the influence of force applied at a specified point, which were then used to identify the frequency values and modal shapes for each of the tested samples. Tables 3, 4 and 5 summarise the frequencies identified for each excitation point. In each tested specimen, applying force at point 27-Z leads to a much larger number of identified frequencies compared to the other two points of excitation. The reason for this is that an impact on the corner leads to the excitation of torsional vibrations, which is not so clearly visible when a load is applied at points located on the axis of plate symmetry due to insufficient excitation energy supplied by the impacts at points 14-Z and 26-Z, which in turn results in the inability to identify some mode shapes. However, this observation is important from the point of view of developing an analytical model of the plate, which is planned in the course of further research. It indicates which modal shapes are clearly identifiable during impacts on particular plate areas, which consequently point to which modes should participate in the multimodal response of the system in specific cases of force application. Therefore, it was decided to leave the empty fields in Tables 3–5 to specify which modes could not be identified for a given excitation.

The results presented in Tables 3–5 show that the greater the thickness of the tested specimen, the fewer frequencies are identified up to 1000 Hz and the higher the fundamental vibration frequency. This relationship is expected, as it results

Table 3. Frequencies of natural vibrations for plate 400 × 800 × 4 mm

Excitation point:		Excited modes																		
		1	2	3	4	5	6	7	8	9	10	11	12	13	14	15	16	17	18	19
14-Z	f_{exp} [Hz]	31.7			89.2	131.4		156.6	175.4	218.8		287.3	305.8		402.8	442.2		532.5	607.1	683.1
26-Z		31.7			89.2	131.5		156.5	175.8	218.8		287.3	305.9		402.8	441.9		532.5		683.0
27-Z		31.7	38.8	87.5	89.3	131.4	150.8	156.6	175.2	218.8	235.3	287.4	305.7	350.9	402.8	442.1	500.5	532.4	606.7	684.0

Note: (grey area) – fields marked in grey indicate that these mode shapes could not be identified.

Table 4. Frequencies of natural vibrations for plate 400 × 800 × 8 mm

Excitation point:		Excited modes														
		1	2	3	4	5	6	7	8	9	10	11	12	13	14	15
14-Z	f_{exp} [Hz]	69.4			190.5	278.4			372.8	459.7		615.4	638.9		850.5	932.9
26-Z		69.4			190.5	278.4		329.4	372.8	459.7		615.5	638.9		850.6	932.5
27-Z		69.4	87.5	190.4	190.6	278.4	326.5	329.1	372.8	459.7	509.1	615.6	638.9	749.9	850.5	933.4

Note: (grey area) – fields marked in grey indicate that these mode shapes could not be identified.

Table 5. Frequencies of natural vibrations for plate 400 × 800 × 12 mm

Excitation point:		Excited modes											
		1	2	3	4	5	6	7	8	9	10	11	12
14-Z	f_{exp} [Hz]	103.5			285.7	422.8		499.7	562.7	692.5		923.9	963.2
26-Z		103.5			285.7	422.8		499.8	562.7	692.6		923.9	963.1
27-Z		103.5	129.0	284.1	285.7	422.8	489.1	499.9	562.7	692.8	763.6	924.4	963.1

Note: (grey area) – fields marked in grey indicate that these mode shapes could not be identified.

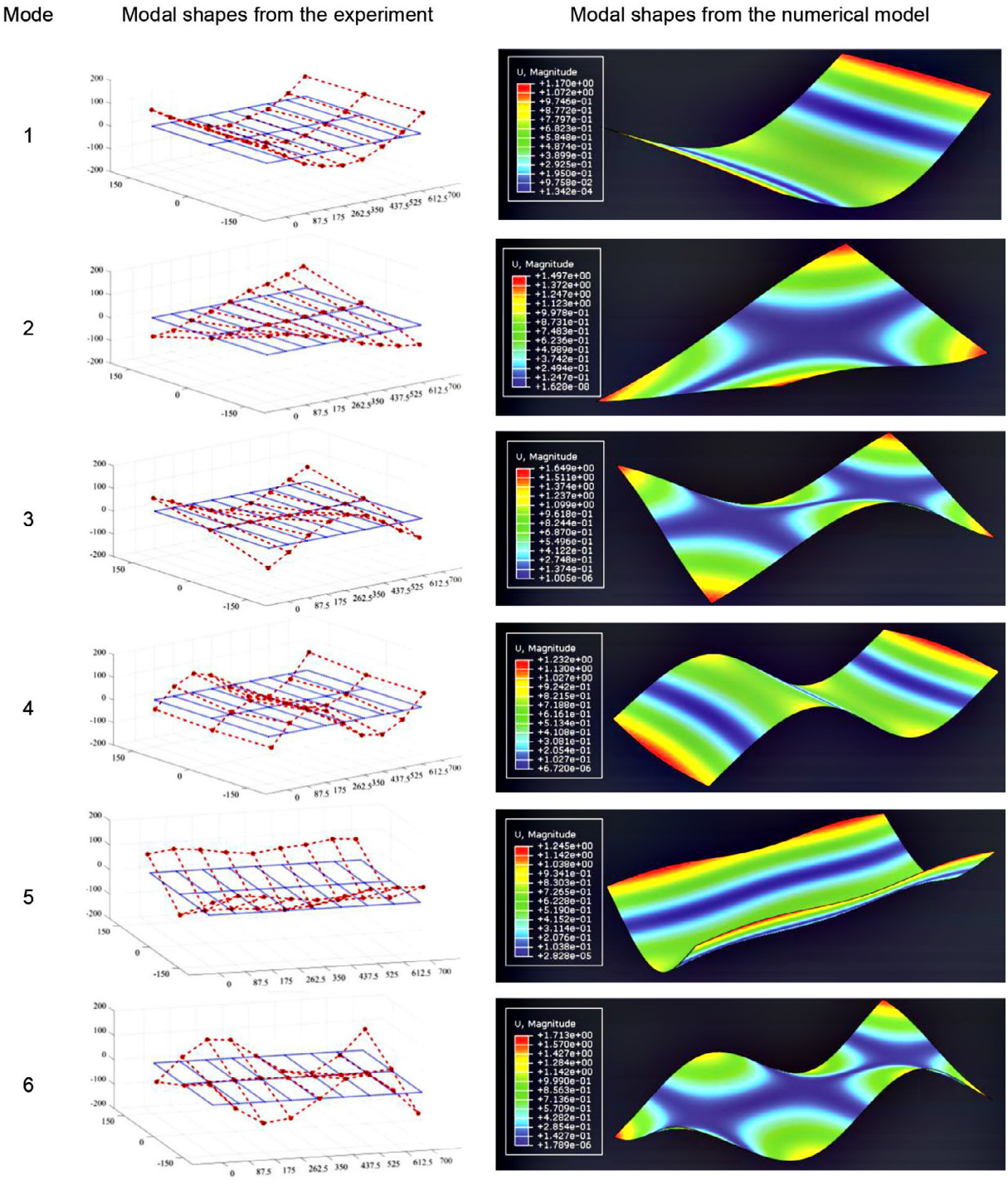

Figure 8. The modal shapes of plate 400 × 800 × 4 mm obtained from the experimental test and the numerical shell model

from the increasing stiffness of the examined glass pane. In the case of samples with nominal thicknesses of 8 and 12 mm, all modes up to 1000 Hz were identified, whereas for the thinnest plate, only the first 19 modes were detected because the high density of modes for the thin plate limits their clear identification.

Comparison between experimental and numerical results

In the next step, the experimental results were compared with those obtained from numerical models composed of shell or solid elements with a mesh size of 4 × 4 mm. Since the focus was on comparing not only the frequency values but also the modal shapes, the experimental results obtained from excitation at point 27-Z were used for the further analysis, as they provided the highest number of identifiable frequencies. For plates with nominal thicknesses of 4 mm and 8 mm, regardless of the finite element type (S4 or C3D8I), the number of modal shapes obtained in both models was the same and higher than those identified experimentally. For this reason, the modal shapes derived from the experiment and numerical models were compared to verify the frequencies corresponding to individual modes for each of the considered sample, as presented for selected cases in Figure 8. The analysis of the natural modal shape diagrams shown in Figure 8 allows the identification of the following vibration modes: the first and fourth natural modes are characterised by longitudinal flexural behaviour, the second, third, and sixth modes by longitudinal torsional behaviour, and the fifth mode by transverse flexural behaviour.

In the next step, the consistency of modal shapes corresponding to individual frequencies obtained on the basis of the experiment and numerical models was verified. The verification was carried out using the MAC. In this process, for each analysed plate, the experimental results obtained from the application of force at point 27-Z were compared, separately with the numerical models built from shell S4 elements and those from the solid C3D8I model. This comparison yields a square matrix and the results are presented in Figures 9–11.

As can be seen, the values obtained on the main diagonal are close to one, indicating a good agreement of the results, while the remaining matrix elements are close to 0. This pattern holds true for both the shell and solid models and can be observed for each glass plate. However, for solid models, the obtained MAC values are slightly higher, which indicates that C3D8I elements represent the modal shapes more accurately. For the thinnest sample (Figure 9), the lowest MAC values were observed for the highest modes, but the MAC remains above 0.879. For the plate 400 × 800 × 8 mm (Figure 10) the lowest value of the MAC is for the third mode, which represents the longitudinal flexural behavior. The thickest plate showed the best agreement in modal shapes between the numerical model and the experiment as presented in Figure 11. This supports the earlier general conclusion that as the thickness of the glass plate increases, the differences between the experimental and numerical modal analysis results decrease.

After confirming that the corresponding modal shapes from the numerical model were consistent with those obtained experimentally, in the final step of the research the percentage differences between the frequency values determined according to Equation 2. were verified. Figure 12 shows the obtained results for the plate with the nominal thickness of 4 mm. As shown, the numerical frequency results are almost identical, regardless of the finite element used. However, among all the tested samples, this pane exhibits the largest discrepancies compared to the experiment, reaching 5.73% for the torsional second mode presented in Figure 8 (Mode 2). These significant differences between the numerical model and the modal analysis for the thinnest glass plate may result from the surface waviness formed during the manufacturing process, which causes local variations in plate thickness, an effect that significantly influences the experimentally obtained frequency values.

An analysis of the results presented in Figure 13 and Figure 14 indicates that as the thickness of the analyzed plate increases, the maximum percentage differences between the numerically and experimentally obtained results decrease, reaching 2.76% and 1.88% for models with nominal thicknesses of 8 and 12 mm, respectively. This may also be related to manufacturing effects and the fact that the greater glass thickness leads to reduced surface waviness, resulting in smaller variation in glass thickness within a single pane. With increasing thickness, there is also a decrease in the accuracy of the numerical results of higher frequencies obtained for

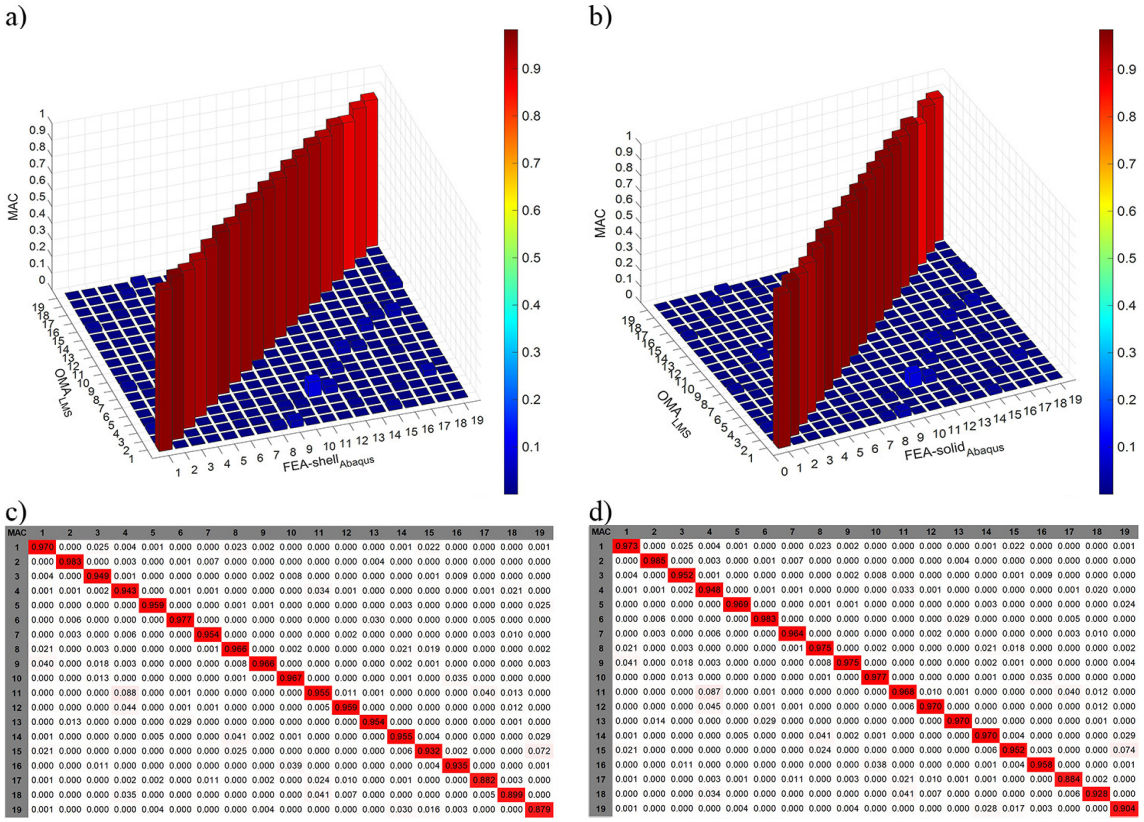

Figure 9. MAC for plate 400 × 800 × 4 mm: (a) graph for shell model; (b) graph for solid model; (c) matrix for shell model; (d) matrix for solid model

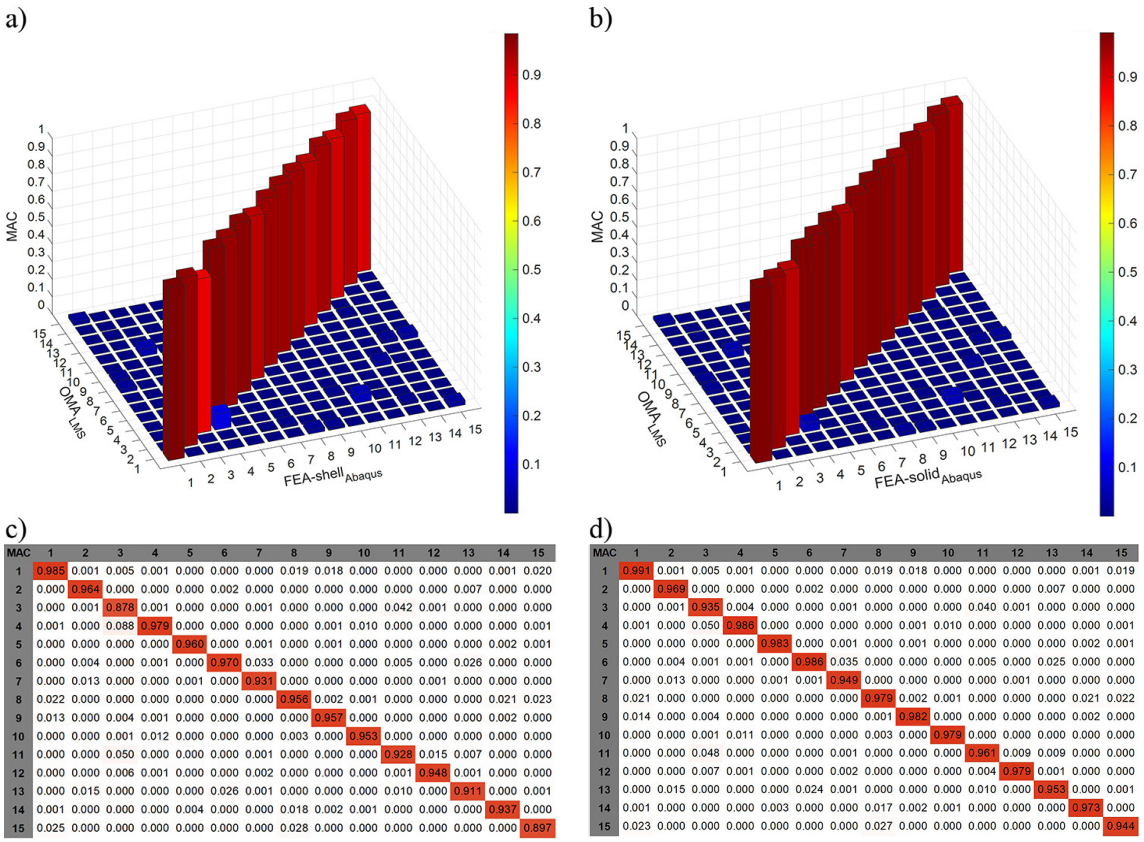

Figure 10. MAC for plate 400 × 800 × 8 mm: (a) graph for shell model; (b) graph for solid model; (c) matrix for shell model; (d) matrix for solid model

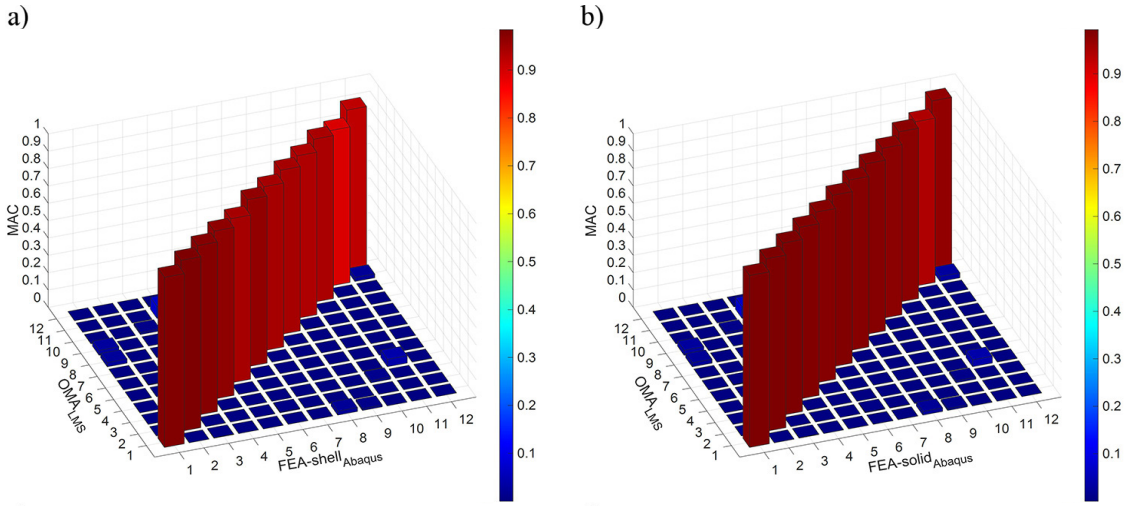

c) MAC	1	2	3	4	5	6	7	8	9	10	11	12
1	0.980	0.000	0.001	0.000	0.001	0.000	0.000	0.024	0.028	0.000	0.000	0.000
2	0.000	0.984	0.000	0.000	0.000	0.004	0.000	0.000	0.000	0.000	0.000	0.000
3	0.002	0.000	0.976	0.001	0.000	0.000	0.000	0.000	0.000	0.011	0.000	0.000
4	0.000	0.000	0.001	0.967	0.000	0.001	0.000	0.000	0.000	0.000	0.068	0.002
5	0.000	0.000	0.000	0.000	0.945	0.000	0.000	0.001	0.000	0.000	0.000	0.000
6	0.000	0.005	0.000	0.000	0.000	0.962	0.000	0.000	0.000	0.000	0.006	0.000
7	0.000	0.002	0.000	0.000	0.000	0.000	0.944	0.000	0.000	0.000	0.000	0.001
8	0.022	0.000	0.000	0.000	0.000	0.000	0.000	0.946	0.001	0.000	0.000	0.000
9	0.010	0.000	0.001	0.000	0.000	0.000	0.000	0.003	0.936	0.000	0.000	0.000
10	0.000	0.000	0.012	0.000	0.000	0.000	0.000	0.000	0.000	0.938	0.000	0.000
11	0.000	0.000	0.000	0.042	0.000	0.000	0.000	0.000	0.000	0.000	0.895	0.007
12	0.000	0.000	0.000	0.001	0.000	0.000	0.001	0.000	0.000	0.000	0.022	0.920

d) MAC	1	2	3	4	5	6	7	8	9	10	11	12
1	0.990	0.000	0.001	0.000	0.001	0.000	0.000	0.023	0.028	0.000	0.000	0.000
2	0.000	0.993	0.000	0.000	0.000	0.004	0.000	0.000	0.000	0.000	0.000	0.000
3	0.003	0.000	0.991	0.001	0.000	0.000	0.000	0.000	0.000	0.000	0.011	0.000
4	0.000	0.000	0.001	0.989	0.000	0.001	0.000	0.000	0.000	0.000	0.067	0.003
5	0.000	0.000	0.000	0.000	0.983	0.000	0.000	0.001	0.000	0.000	0.000	0.000
6	0.000	0.005	0.000	0.000	0.000	0.987	0.001	0.000	0.000	0.000	0.007	0.000
7	0.000	0.002	0.000	0.000	0.000	0.000	0.982	0.000	0.000	0.000	0.000	0.001
8	0.021	0.000	0.000	0.000	0.000	0.000	0.000	0.983	0.001	0.000	0.000	0.000
9	0.011	0.000	0.001	0.000	0.000	0.000	0.000	0.003	0.979	0.000	0.000	0.000
10	0.000	0.000	0.011	0.000	0.000	0.000	0.000	0.000	0.000	0.981	0.000	0.000
11	0.000	0.000	0.000	0.039	0.000	0.001	0.000	0.000	0.000	0.000	0.946	0.004
12	0.000	0.000	0.000	0.002	0.000	0.001	0.001	0.000	0.000	0.000	0.029	0.973

Figure 11. MAC for plate 400 × 800 × 12 mm: (a) graph for shell model; (b) graph for solid model; (c) matrix for shell model; (d) matrix for solid model

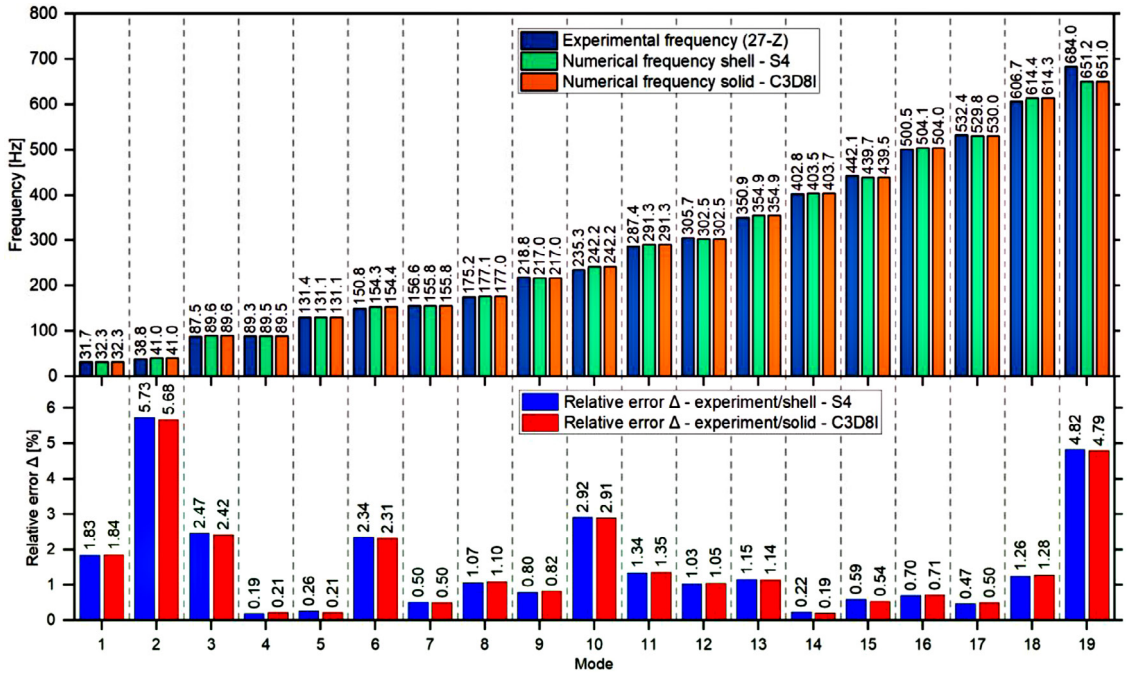

Figure 12. Differences in frequency values with regard to experiment for plate 400 × 800 × 4 mm

shell models compared to the solid ones. This may be due to the fact that dividing the plate by thiskness in the case of C3D8I elements better reflects the deformation of a given modal shape. On the other hand, the differences between the two numerical models are less than 0.5%, and shell elements require over an order of magnitude less computation time in this case, which

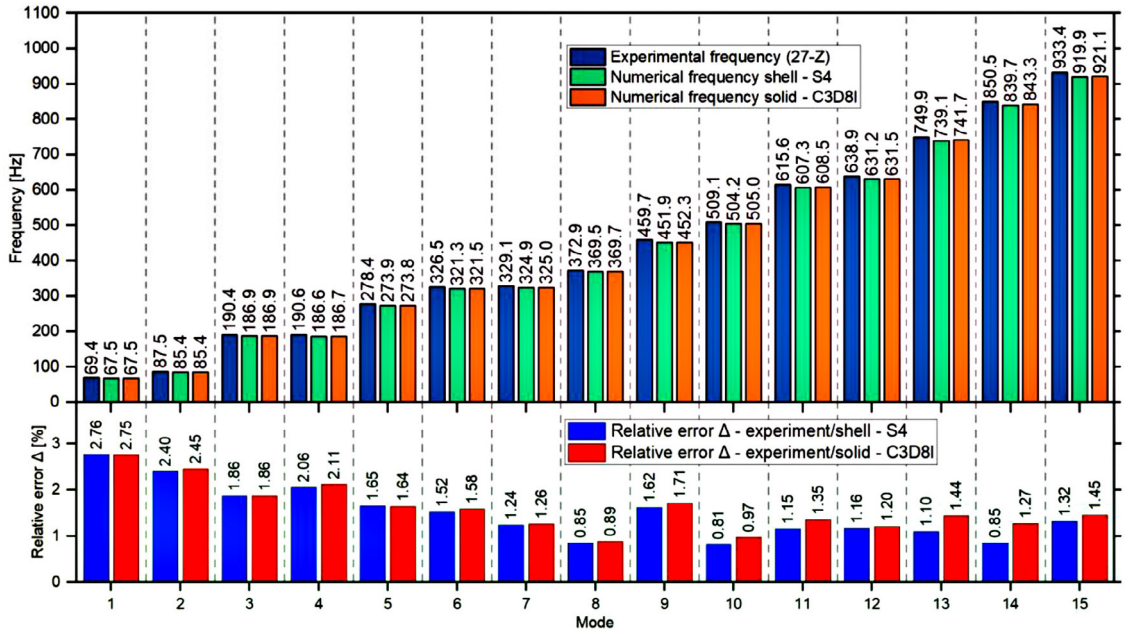

Figure 13. Differences in frequency values with regard to experiment for plate 400 × 800 × 8 mm

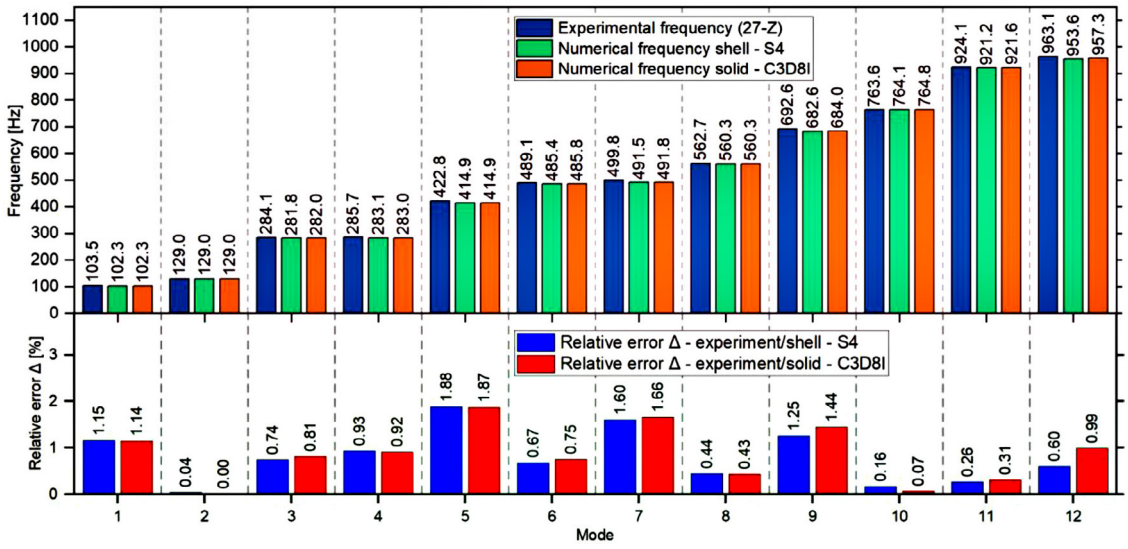

Figure 14. Differences in frequency values with regard to experiment for plate 400 × 800 × 12 mm

should be taken into account when selecting a numerical model type.

CONCLUSIONS

In this study, an experimental modal analysis was performed on three glass samples of different thicknesses. Thickness measurements taken during the tests showed that as the thickness of the plate increases, its deviation from the nominal dimension (specified by the manufacturer) decreases. This may be related to the toughening process, which sometimes leads to surface waviness in very thin plates. However, tests carried out on various samples showed that thickness has a significant impact on the numerical results of dynamic characteristics obtained from the model. Therefore, for thin plates, this parameter should be carefully verified and considered in the computational process. In the next step of the research, based on the acceleration values obtained at 27 points under the excitation applied by a modal hammer, the frequency values and corresponding modal shapes were identified for each individual sample. The results obtained

from the tests were compared with those from numerical models made of S4 shell and C3D8I solid elements. For both types of numerical models, a convergence analysis was performed to determine when the mesh refinement ceases to have a significant impact on the results obtained. The analyses carried out showed that the minimum mesh size that allows for obtaining differences in results between adjacent models below 1% is approximately equal to the thickness of the glass plate, which, given their small values, leads to a significant degree of mesh density. However, for thicker plates, it is worth reducing the mesh size further in order to obtain results that are closer to reality, therefore, the convergence analysis of the numerical model should be performed each time for the case under analysis.

The comparison of results showed that both the shell and solid elements used in numerical models exhibit very good agreement with the experimental data, with the former requiring significantly less computation time. For selected glass plates, the required time was approximately ten times shorter. This leads to the general conclusion that in the case of modal analysis of glass panes, where frequency values and modal shapes are sought, the use of shell elements is sufficient to obtain reliable results, and at the same time seems to be the optimal solution, significantly reducing the computational cost. The above conclusion does not apply to dynamic tests on glass plates, including the analysis of displacements or stresses under impact or other form of excitations, as these aspects require additional study and will be the subject of further research.

However, the results obtained during the experiment are crucial for the correct description of the analytical model of the dynamic multimodal response of a glass plate subjected to an impulse load, which is planned in further work. The research shows that applying the force at the corner of the plate provides the energy to the widest spectrum of modal shape excitation and at the same time indicates which modal shapes cannot be identified during sudden impact in the centre of the plate or on its axis of symmetry. In further work, research is planned to determine whether this behaviour can be used to simplify the analytical model for the dynamic analysis of a glass plate.

REFERENCES

1. Fu Z.F., He J. Modal Analysis. 1st ed. Elsevier, Butterworth-Heinemann, 2001.
2. Tan M.H.M.A., Lile N.L.T., Mat F., Yaacob S. Elastic characterization of glass by modal analysis. International Journal on Advanced Science, Engineering and Information Technology 2012, 2(3), 224–226. https://doi.org/10.18517/IJASEIT.2.3.191
3. Chaparala S., Xue L., Yu D., Park S. Dynamics behavior of flat glass panels under impact conditions: Experiments and numerical modeling. Journal of the Society for Information Display 2015, 23, 3, 97–106. https://doi.org/10.1002/JSID.283
4. Fröling M., Persson K., Austrell P.E. A reduced model for the design of glass structures subjected to dynamic impulse load. Engineering Structures 2014, 80, 53–60. https://doi.org/10.1016/J.ENGSTRUCT.2014.08.043
5. Bedon C., Fasan M., Amadio C. Vibration analysis and dynamic characterization of structural glass elements with different restraints based on operational modal analysis. Buildings 2019, 9(1), 13. https://doi.org/10.3390/BUILDINGS9010013
6. Bedon C., Bergamo E. Vibration experiments for diagnostic investigations on a glass suspension footbridge. Vibroengineering Procedia 2019, 24, 41–46.. https://doi.org/10.21595/VP.2019.20612
7. Bedon C., Amadio C. Glass facades under seismic events and explosions: a novel distributed-TMD design concept for building protection. Glass Structures and Engineering 2018, 3(2), 257–274. https://doi.org/10.1007/S40940-018-0058-9/TABLES/3
8. Bedon C., Amadio C. Numerical assessment of vibration control systems for multi-hazard design and mitigation of glass curtain walls. Journal of Building Engineering 2018, 15, 1–13. https://doi.org/10.1016/J.JOBE.2017.11.004
9. Hála P., Zemanová A., Plachý T., Konrád P., Sovják R. Experimental modal analysis of glass and laminated glass large panels with EVA or PVB interlayer at room temperature. Materials Today: Proceedings. 2022, 62, 2421–2428. https://doi.org/10.1016/J.MATPR.2022.02.578
10. Jeong Y., Jeon Y., Lee W., Yoon J. Development of an equivalent analysis model of PVB laminated glass for TRAM crash safety analysis. Polymers 2025, 17, 25. https://doi.org/10.3390/POLYM17010025
11. Figuli L., Papan D., Papanova Z., Bedon C. Experimental mechanical analysis of traditional in-service glass windows subjected to dynamic tests and hard body impact. Smart Structures and Systems. 2021, 27, 365–378. https://doi.org/10.12989/SSS.2021.27.2.365
12. Lenk P., Coult G. Damping of Glass Structures and

Components. In Challenging Glass 2, Proceedings of the Conference on Architectural and Structural Applications of Glass, TU Delft, Delft, The Netherlands, 20–21 May 2010. www.eckersleyocallaghan.com

13. Haldimann M., Luible A., Overend M. Structural engineering document, structural use of glass. IABSE. 2008, 10.
14. EN 572-1:2016 Glass in building - Basic soda-lime silicate glass products - Part 1: Definitions and general physical and mechanical properties.
15. Le Bourhis E. Glass: Mechanics and Technology. John Wiley & Sons, 2014.
16. Biolzi L., Bonati A., Cattaneo S. Laminated glass cantilevered plates under static and impact loading. Advances in Civil Engineering 2018, 1, 7874618. https://doi.org/10.1155/2018/7874618
17. Biolzi L., Cattaneo S., Simoncelli M. Post-failure behavior of 2-ply laminated glass plates with different interlayers. Engineering Fracture Mechanics 2022, 268, 108496. https://doi.org/10.1016/J.ENGFRACMECH.2022.108496
18. PN-EN 16612:2020 Glass in building - Determination of the lateral load resistance of glass panes by calculation.
19. Kozłowski M., Zemła K., Kosmal M., Kopyłow O. Experimental and FE study on impact strength of toughened glass–retrospective approach. Materials 2021, 14, 7658. https://doi.org/10.3390/ma14247658
20. Bocheński M., Gawryluk J., Kłoda Ł. Experimental modal analysis of an active thin-walled composite structure. Modelling, Measurement and Control B 2019, 88, 2–4. https://doi.org/10.18280/MMC_B.882-415
21. Jarosińska M., Berczyński S. Changes in frequency and mode shapes due to damage in steel–concrete composite beam. Materials 2021, 14(21), 6232. https://doi.org/10.3390/MA14216232
22. Shabani A., Feyzabadi M., Kioumarsi M. Model updating of a masonry tower based on operational modal analysis: The role of soil-structure interaction. Case Studies in Construction Materials 2022, 16, 00957. https://doi.org/10.1016/J.CSCM.2022.E00957
23. Kim CJ. Comparison of mode shapes of carbon-fiber-reinforced plastic material considering carbon fiber direction. Crystals 2021, 11, 311. https://doi.org/10.3390/cryst11030311
24. Chybiński M., Szewczyk P., Abramowicz M., Polus Ł. Vibration behaviour of aluminium-timber composite beams. Engineering Structures 2025, 343, 120989. https://doi.org/10.1016/J.ENGSTRUCT.2025.120989
25. Heiskari J., Romanoff J., Laakso A., Ringsberg JW. On the thickness determination of rectangular glass panes in insulating glass units considering the load sharing and geometrically nonlinear bending. Thin-Walled Structures 2022, 171, 108774. https://doi.org/10.1016/J.TWS.2021.108774
26. Griffith J., Marinov V., Marinitsh S., Teich M. Structural analysis of folded glass plate structures. In: Belis J, Bos F, Louter C, eds. Challenging Glass 5 – Conference on Architectural and Structural Applications of Glass. Ghent University 2016, 361-370. https://doi.org/10.7480/cgc.5.2226
27. Simulia, Abaqus Computer Software, Providence, RI, USA, 2014.